CMST 31(1) 5–11 (2025) DOI:10.12921/cmst.2024.0000025

Lyapunov Instability in Cell Models With and Without Time-Reversible Heat Transfer

Wm.G. Hoover[1], C.G. Hoover[2]

2870 Ruby Vista Drive, Unit 109
Elko, Nevada 89801, USA
[1]*E-mail: hooverwilliam@yahoo.com*
[2]*E-mail: hoover1carol@yahoo.com*

Received: 31 December 2024; accepted: 22 January 2025; published online: 9 March 2025

Abstract: Two-temperature pedagogical cell models, extensions of the equilibrium Einstein model of solid state physics, can allow nonequilibrium hot-to-cold heat transfer. These heat-flow models can be driven by thermostatted temperature differences, for instance between horizontal and vertical degrees of freedom. We present pedagogical benchmark Lyapunov exponents for four equilibrium cell models: isoenergetic Hamiltonian, constrained Isokinetic, and two Isothermal Nosé-Hoover models. We also compute representative Lyapunov exponents for two members of a family of two-temperature *dissipative* Nosé-Hoover cell models. Further exploration of such dissipative models is the subject of the 2024–2025 $1000 Snook Prize.

Key words: cell model, fractals, Lyapunov exponents, heat transfer, Snook Prize, λ, time reversibility

I. Molecular Dynamics and Equilibrium Cell Models

Berni Alder and Tom Wainwright developed molecular dynamics at the University of California's Livermore Radiation Laboratory in the 1950s [1]. They began with hard disks and hard spheres, making connections with the Boltzmann equation for dilute gases, dense-fluid/solid cell models of Gibbs' thermodynamics, and the melting/freezing transition of dense fluids and crystalline solids. The two different two-body cell models illustrated in Fig. 1 are related to the Einstein and Debye models (dating back to 1907 and 1912, respectively) for equilibrium solid state frequency distributions. The models turn out to closely reproduce the isothermal pressure-volume dependence for the hard-disk melting/freezing phase transition [2]. These results took advantage of the simplicity of instantaneous hard-particle collisions obtained with the aid of classical Newtonian dynamics. For more "realistic" pair interactions the equations of state linking pressure P, volume V, energy E, and temperature T could be obtained as applications of the virial theorem's linking of microscopic collisions to the macroscopic pressure.

Away from equilibrium the shear and bulk viscosities and thermal conductivity were formulated as theoretically based "transport coefficients" derived from Boltzmann's kinetic theory or Green and Kubo's linear-response theory. Gibbs' statistical mechanics relates thermodynamic properties to derivatives of the "free energies", Helmholtz' $A(V,T)$ and Gibbs' $G(P,T)$, obtained by integrating phase-space probabilities over N-body spaces in the limit where N is macroscopic.

In the opposite few-body limit, where a single particle moves at constant energy in a potential field due to its fixed neighbors, Gibbs' or Helmholtz' many-body phase integral can be approximated by the Nth power of a one-body integral. Two one-body examples are illustrated in the "cell model(s)" of Fig. 1. It is remarkable that this simple idea can be usefully extended to provide an even more nearly accurate model, the *correlated cell model*. That model [2] incorporates the sliding of rows of particles seen earlier in computer-generated movies. In the correlated cell model melting occurs as a consequence of sufficient area expansion (to 4/3 the close-packed area) to allow parallel rows of particles to shear past their neighbors.

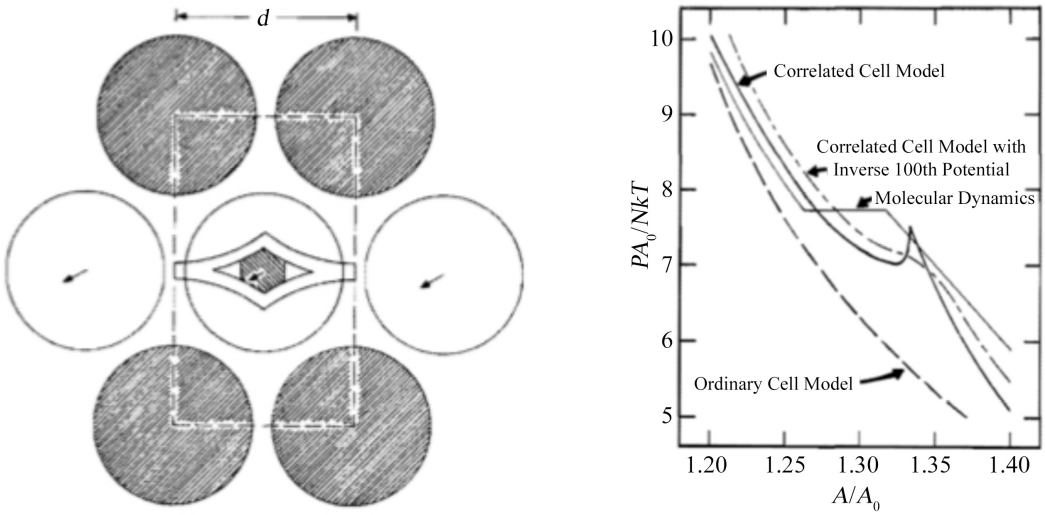

Fig. 1. Equilibrium Cell Models (on the left) and Pressure-Area Isotherms (on the right) for Hard Disks. On the left (the center of) a central "wandering" hard-disk particle can explore the tiny hexagonal shaded area as the wanderer interacts with six fixed neighbors in the ordinary cell model. In the *correlated cell model* only the four darkly shaded particles bound the central particle's motion. In this correlated model the leftmost and rightmost disks act as moving periodic images of the central open-circle particle. Pressures in the figure are calculated from both cell models, manybody molecular dynamics, and the inverse 100th power potential using Gibbs' statistical mechanics, as is described in Ref. 2

II. Isoenergetic Mechanics at Constant Total Energy

The present work was inspired by the cell-model examples of Fig. 1. We intend the numerical results in the eight figures that follow here to serve as benchmarks for those developing computer simulations using straightforward Hamiltonian mechanics or its more recent Isokinetic and Nosé-Hoover modifications with thermostat forces added to the motion equations. Fig. 2 serves as an excellent pedagogical example, with plenty of fine structures in the relatively long-time trajectory shown there. With a correctly programmed solution using a fourth-order Runge-Kutta integrator the reader should have little difficulty duplicating the million-timestep trajectory shown as Fig. 2.

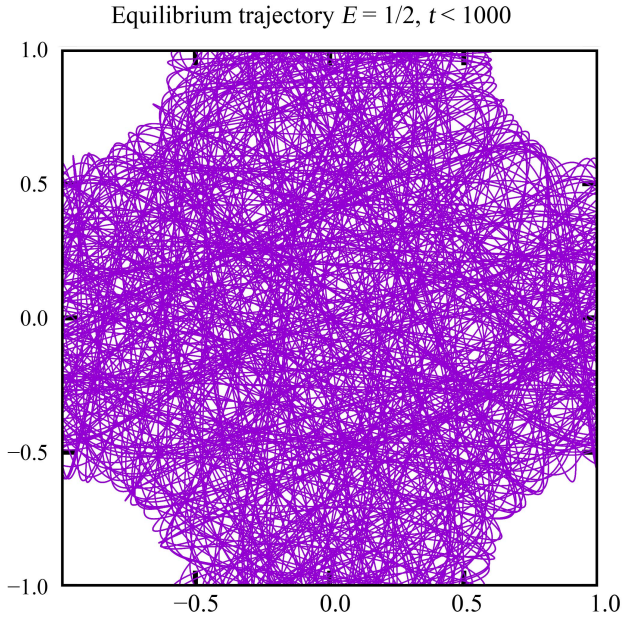

Fig. 2. Hamiltonian mechanics with initial conditions $(x, y, p_x, p_y) = (0, 0, 0.6, 0.8)$ and one million fourth-order Runge-Kutta timesteps, $(dt = 0.001)$. The wanderer particle interacts with four particles fixed at $(x, y) = (\pm 1, \pm 1)$. The interaction potential with the four fixed particles is $\phi = (1 - r^2)^4$ for $r < 1$ and vanishes outside that range

Although there are many integrators ranging from second order to eighth order, or even more, we settled on the simplicity of the fourth-order Runge-Kutta after considerable exploration of many alternatives. Fig. 3 furnishes an illuminating example. For clarity it compares integrations using four values of the Runge-Kutta timestep, $0.001, 0.002, 0.005$, and 0.010. The underlying cell model is the same as that shown in Figs. 1 and 2: a wanderer particle moves in a 2×2 square, interacting with four fixed particles at $(x, y) = (\pm 1, \pm 1)$ with the smooth short-ranged pair potential $\phi(r) = (1 - r^2)^4$.

III. Extensions of Hamiltonian Mechanics

Nosé's 1984 work [3, 4] revolutionized Isoenergetic molecular dynamics and helped create nonequilibrium molecular dynamics. "Isokinetic" mechanics constrains the kinetic energy, $(p_x^2 + p_y^2)/2$. A straightforward application of Gauss' Principle (of "Least Constraint") leads to new motion equations. Choosing the mass and relaxation time of the constraint forces equal to unity, the Isokinetic condition is built into the motion equations:

$$\dot{p} = F - \zeta p \; ; \; \zeta = (F \cdot p)/(p \cdot p) \; [\text{Gaussian Isokinetic}].$$

The "Nosé-Hoover" version of Nosé's work [5] also follows this friction-coefficient form, but with a separate differential equation for the coefficient ζ:

$$\dot{p} = F - \zeta p \; ; \; \dot{\zeta} = (p^2 - T)/\tau \text{ [Nosé-Hoover Isothermal]}.$$

A similar version, which we also explore here, controls p_x^2 and p_y^2 separately, with two friction coefficients, ζ_x and ζ_y.

To sum up, we consider the Hamiltonian and Isokinetic models with four motion equations plus two additional Nosé-Hoover models, with five and six motion equations, with the two-coefficient model applicable both at equilibrium, with two equal temperatures, and at nonequilibrium, where the two temperatures differ and drive a hot-to-cold heat flux.

The last nonequilibrium case provides an example of irreversible flows from reversible motion equations. We choose to study the pedagogical Lyapunov spectrum of dynamical λ stability coefficients to benchmark all of these models, describing them in the next section.

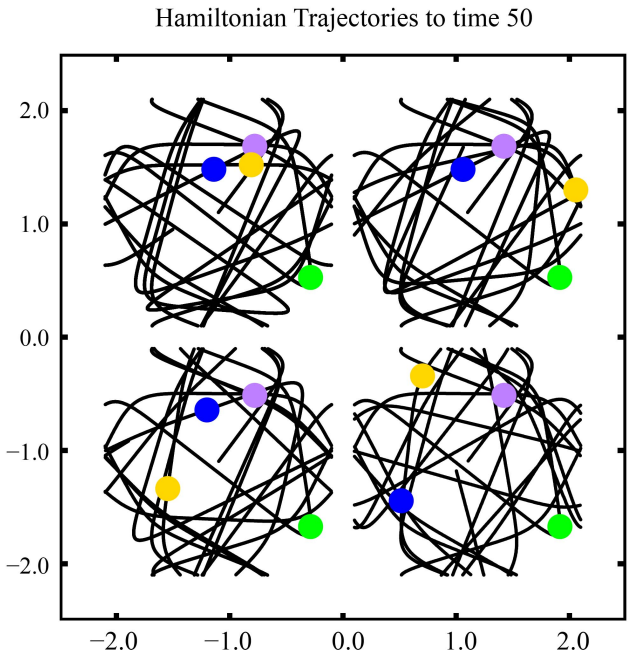

Fig. 3. Four wanderer-particle trajectories with $dt = 0.001$ (top left), 0.002 (top right) , 0.005 (bottom left), 0.010 (bottom right) emphasizing points at times of 10 (purple), 20 (green), 30 (blue), 40 (gold) with periodic boundaries in the x and y directions. The initial condition is $p = (0.6, 0.8)$ with $(x, y) = (0, 0)$. The total energy agrees with the initial to eleven-figure accuracy at the conclusion of the run, time = 50. Despite this accurate energy the trajectories differ markedly at time 40. The maximum potential energy of $1/2$ occurs along four quarter-circles centered at $(\pm 1, \pm 1)$ with radii $0.398878 = \sqrt{1 - 2^{-1/4}}$. In the figure, for comparison purposes the top row of trajectories are displaced by $(\mp 1.1, +1.1)$ and the bottom row by $(\mp 1.1, -1.1)$ Each of the four trajectories was generated for a maximum time of 50. Visually, the four purple and green trajectories agree, unlike the blue (0.005) and gold (0.010) points at times 30 and 40

IV. Lyapunov Spectra for Three Equilibrium Cell Models

In this work we augment standard isoenergetic Hamiltonian simulations with Isokinetic as well as two equilibrium and nonequilibrium versions of Nosé-Hoover isothermal mechanics. We focus on the Lyapunov spectrum to characterize all four of these cell-model types(Hamiltonian, Isokinetic, and two versions of Nosé-Hoover dynamics).

We use fourth-order Runge-Kutta integration for all of the problems in this work. Experimentation with various timesteps and fifth-order methods [6] shows that a fourth-order solution with time steps 0.001 or 0.002 provides reliable numerical data. Larger timesteps, 0.005 or 0.010, provide inaccuracy, as indicated by the gold disks of Fig. 3, which was carried out to a maximum time of 50.

Around 1980, with the new tool of nonequilibrium molecular dynamics, it was discovered that time-reversible, but dissipative, simulations (with gradients in density, velocity, or temperature) lead to fractional dimensional "fractal" phase-space distributions [7, 8]. The time-reversed simulations turned out to be "unstable". The instability can be best characterized with the Lypunov spectrum of exponents, which describe the expansion/unstable or contraction/stable of phase-space distributions, one for each dimension. The spectra for Hamiltonian mechanics are composed of equal numbers and magnitudes of Lyapunov exponents, $\{\pm\lambda\}$ corresponding to Liouville's Theorem that classical time-reversible mechanics conserves phase-space volume. Numerical algorithms for the spectrum are based on the exponential growth or decay rates of n-dimensional phase-space volumes, starting with the growth of a line

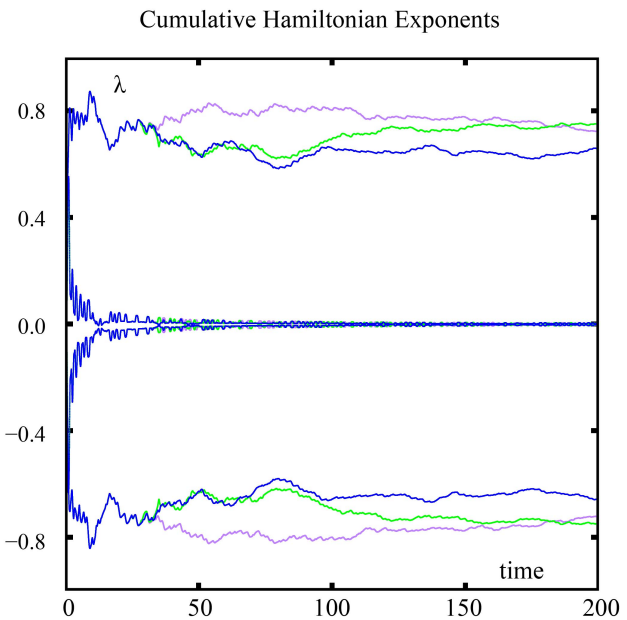

Fig. 4. Longer calculations of the four Hamiltonian Lyapunov exponents with $dt = 0.001$ (purple), 0.002 (green) and 0.005 (blue). Here the initial conditions in the four-dimensional phase space are $(x, y, p_x, p_y) = (0, 0, 0.6, 0.8)$

segment, as $e^{\lambda_1 t}$, of an area, as $e^{[\lambda_1+\lambda_2]t}$, and of a volume, as $e^{[\lambda_1+\lambda_2+\lambda_3]t}$. The Hamiltonian cell model has four Lyapunov exponents as the motion takes place in a four-dimensional space, (x, y, p_x, p_y).

Fig. 4 illustrates the two larger Lyapunov exponents for the continuous Hamiltonian cell model of Figs. 2 and 3, carried out to a time of 200 with Runge-Kutta integration. The good agreement between the two smaller timesteps, 0.001 and 0.002, indicates that either choice is satisfactory. Shimada and Nagashima [9], as well as Benetinne's group [10], developed algorithms well-suited to the computation of Lypunov exponents, with λ_1 above and λ_2 below, as shown in Fig. 4. See also our work with several colleagues and students [11–13].

Fig. 5 shows the four Isokinetic exponents, one positive and paired with a negative and two vanishing, likewise paired. In every case the initial values for the coordinates and momenta are $\{x, y, p_x, p_y\} = \{0, 0, 0.6, 0.8\}$. Because the forces vanish with the wanderer particle, at or nearby the origin, the initial friction coefficient or coefficients vanish. Just as in the Hamiltonian case the exponents $\pm\lambda$ are paired, $\pm\lambda$ indicating the lack of any long-term phase-volume change. The Nosé-Hoover motion equations come in two varieties, with five-and-six-dimensional phase spaces:

$$\dot\zeta = (p^2 - T)/\tau \text{ [Single Thermostat]},$$

$$\dot\zeta_x = (p_x^2 - T)/\tau \; ; \; \dot\zeta_y = (p_y^2 - T)/\tau \text{ [Double Thermostats]}.$$

The cumulative Lyapunov spectra are illustrated in Figs. 6 and 7.

The present work was undertaken with the goal of better understanding the distributions obtained with *nonequilibrium* versions of the dynamics. A 1991 precursor [12] considered the heat transfer between the horizontal and vertical kinetic temperatures of an anisotropic harmonic oscillator with two friction coefficients, ζ_x and ζ_y, and a different angle-dependent pair potential, expressed here in polar coordinates:

$$\phi = (r^2/2)[1 + 0.5\cos(3\theta)] \; ;$$
$$\dot p_x = F_x - \zeta_x p_x \; ; \; \dot p_y = F_y - \zeta_y p_y \; ;$$
$$\dot\zeta_x = (p_x^2 - T_x)/\tau \; ; \; \dot\zeta_y = (p_y^2 - T_y)/\tau,$$

chosen for its resemblance to the Hénon-Heiles system. This model, with $T_x = 2$ and $T_y = 1/2$ has a six-dimensional Lyapunov spectrum $\{0.117, 0.043, 0.001, -0.008, -0.067, -0.200\}$, indicating a phase-space distribution dimensionality between 5 (growing as $e^{+0.086t}$) and 6 (shrinking as $e^{-0.114t}$) based on the sums of five and six exponents. Exchanging the two temperatures gives $\{0.031, 0.001, -0.005, -0.043, -0.128, -0.216\}$ corresponding to a dimension-

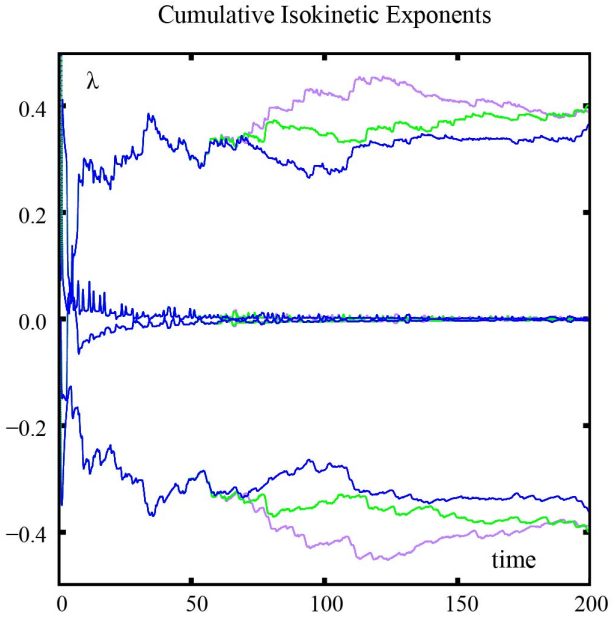

Fig. 5. Four Isokinetic Lyapunov Exponents with $dt = 0.001$ (purple), 0.002 (green), and 0.005 (blue). As usual, the initial condition sets the wanderer at the origin with kinetic energy $(p_x^2 + p_y^2)/2 = = (0.36 + 0.64)/2 = 0.50$, nicely conserved and suggesting that the largest Lyapunov exponent is $\lambda_1 = 0.39 \pm 0.01$ and the smallest, $\lambda_4 = -0.39$ while λ_2 and λ_3 both vanish. The motion equations are $(\dot x, \dot y, \dot p_x, \dot p_y) = (p_x, p_y, F_x - \zeta p_x, F_y - \zeta p_y)$. The friction coefficient ζ is $(F \cdot p)/(p_x^2 + p_y^2)$ and the initial conditions are the usual, $(x, y, p_x, p_y, \zeta) = (0, 0, 0.6, 0.8, 0)$, solved with fourth-order Runge-Kutta integration with up to two hundred thousand points

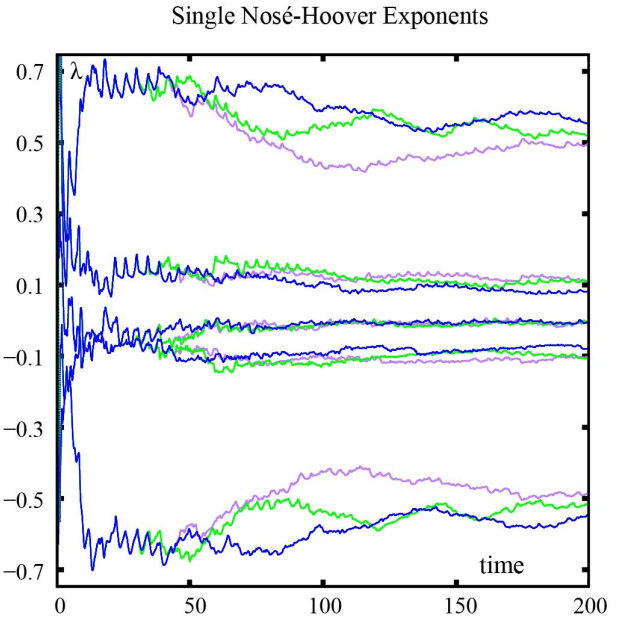

Fig. 6. Four Nosé-Hoover Lyapunov Exponents, $\pm 0.50, \pm 0.11$, are paired with their negatives. There is also a single vanishing exponent. The calculations are compared with $dt = 0.001$ (purple), 0.002 (green), and 0.005 (blue). The Lyapunov data suggest that the largest Lyapunov exponent is $\lambda_1 = 0.50 \pm 0.01$. The motion equations are $(\dot x, \dot y, \dot p_x, \dot p_y, \dot\zeta) = (p_x, \; p_y, \; F_x - \zeta p_x, \; F_y + -\zeta p_y, \; [\, p_x^2 + p_y^2 - 2T \,]/\tau)$. The target temperature T and relaxation time τ are both unity. Again the initial conditions place the wanderer at the origin with $(p_x = 0.6, \; p_y = 0.8, \; \zeta = 0)$. $\dot\zeta = = [\, p_x^2 + p_y^2 \,]/2\tau - K$. The friction coefficient ζ is determined by this last feedback equation for $\dot\zeta$. As usual, the motion equations are solved with fourth-order Runge-Kutta integration

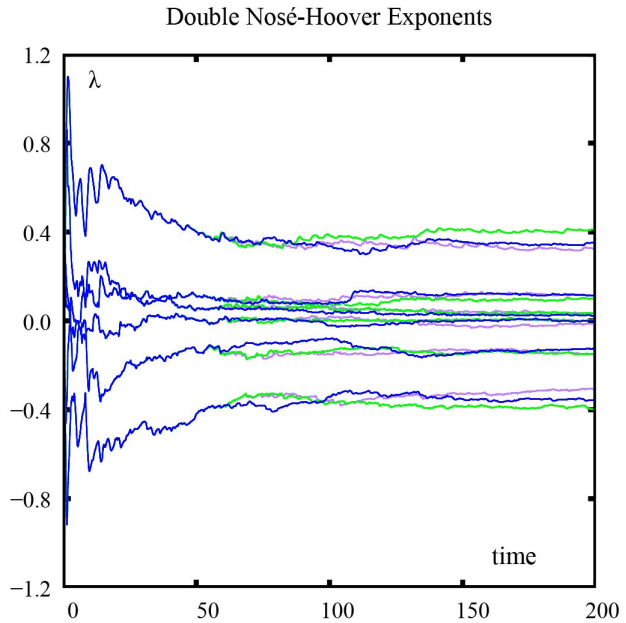

Fig. 7. Here the two Nosé-Hoover momenta are separately controlled with target temperatures T of unity: $\dot{p}_x = F_x - \zeta_x p_x$; $\dot{p}_y = = F_y - \zeta_y p_y$ with $\dot{\zeta}_x = p_x^2 - T$; $\dot{\zeta}_y = p_y^2 - T$. The six motion equations are those of Fig. 6 but with ζ_x and ζ_y both initialized at zero, $p_x,\ p_y = 0.6,\ 0.8$. Just as in the Hamiltonian case this Nosé-Hoover equilibrium system generates a symmetric Lyapunov spectrum with two positive-negative pairs of exponents. There are also two zero exponents

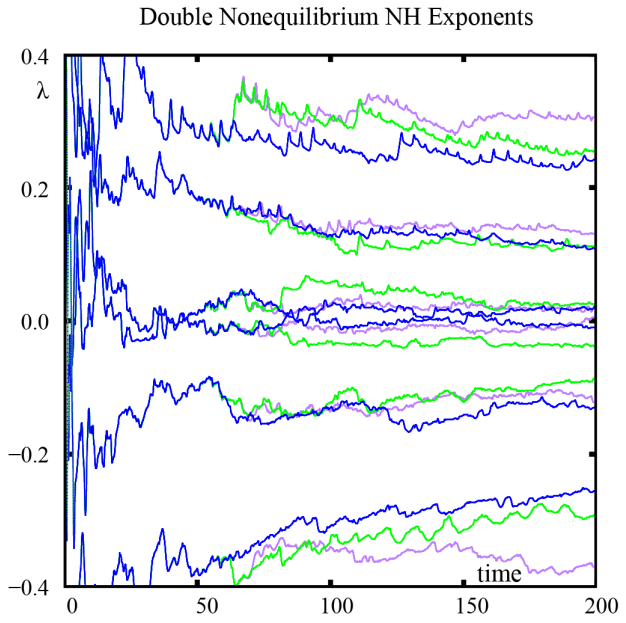

Fig. 8. Unlike all the previous cell-model simulations the horizontal and vertical temperatures here are controlled differently, at 2 and 1/2, respectively. Initially $p_x,\ p_y = 0.6,\ 0.8$. This nonequilibrium, but "time-reversible", system takes advantage of the opportunity to transfer heat from hot to cold, giving a negative sum of the six exponents equal to -0.026:

$$+0.309 + 0.128 + 0.020 + 0.006 - 0.122 - 0.367 = -0.026.$$

Lyapunov instability separates the timestep dependence visually around a time of 60. Permuting the temperatures from 2 and 1/2 to 1/2 and 2 provides a similar spectrum and a smaller sum:

$$+0.312 + 0.112 + 0.008 - 0.014 - 0.109 - 0.317 = -0.008.$$

Initially $p_x = 0.6,\ p_y = 0.8$. More extensive computations suggest that the uncertainties of the exponents for runs to time 200 are roughly ± 0.01. Evidently, these results are consistent with the extended phase-space distribution being *fractal* rather than continuous. Because the last Lyapunov exponent is $\lambda_6 = -0.367$ the dimensionality loss from 6 is $0.026/0.367 \simeq 0.070$ according to Kaplan and Yorke's interpolation recipe [14]. The permuted temperatures also give a tiny estimate for the dimensionality loss, $0.008/0.317 \simeq 0.025$. It is noteworthy that even this simple one-particle model reproduces the symmetry breaking associated with the Second Law of Thermodynamics. Despite the time-reversibility of the motion equations any numerical solution soon follows in the direction of dissipation. A time-reversed simulation, with a positive Lyapunov sum, is numerically unstable. Whether or not the six-dimensional phase-space distribution is ergodic is an interesting subject worthy of investigation. If it is, permuting the momenta and the temperatures (four combinations of initial conditions) should lead to four similar spectra, the first step in applying for the Snook Prize of 2025. We compared the four runs with *200 million* timesteps and found that the cumulative largest Lyapunov exponents were all the same to three figures, $\langle \lambda_1 \simeq 0.293 \rangle$, suggesting that the dynamical distribution *is* ergodic. More details, in the form of a Snook Prize entry, of the temperature dependence of the spectra, are very welcome

ality between 3 (growing as $e^{0.027t}$) and 4 (shrinking as $e^{-0.016t}$).

The complexity of additional manybody thermostatted systems was explored using Nosé-Hoover mechanics in 1993 [13]. Qualitative differences between six-body and eight-body anharmonic chains (with half cold and half hot) could be characterized with special attention to constraints on the satellite trajectories required for the computation of Lyapunov spectra.

Our goal in the present work is to better understand a cell model based on the simple pair potential $\phi(r) = (1 - r^2)^4$ which we used earlier [6] to evaluate the relative usefulness of seven integrators of the four ordinary differential equations for $(\dot{x}, \dot{y}, \dot{p}_x, \dot{p}_y)$. A sample million-timestep equilibrium dynamics, with energy $E = 0.5$ was pictured here in Fig. 2.

The Hamiltonian cell-model dynamics is described with four differential equations. Exploration shows that fourth-order Runge-Kutta integrators provide stability, and despite Lyapunov *instability*, visual trajectory accuracy to a time of 20 or 30 with timesteps of 0.001, 0.002, and 0.005. See Figs. 3 and 4, where the filled disks in Fig. 3 show that the Lyapunov instability degrades solutions with $dt > 0.002$.

V. Summary

Cell models replace the manybody problem [6, 14, 15] with a one-body problem. Despite this simplicity the various approaches we have outlined, augmenting the Hamiltonion description with isokinetic and Nosé-Hoover versions of thermostatting provide pedagogical models for equilibrium and nonequilibrium dynamical systems. The programming

implementing the computation of Lyapunov spectra is somewhat tedious. Carrying out the present work we finally located an error in our version of the Gram-Schmidt algorithm. Finding and correcting this occupied us off and on for two months, culminating with success on Christmas Day 2024. A rough draft manuscript was first submitted to CMST on New Year' Eve 2024, a week later.

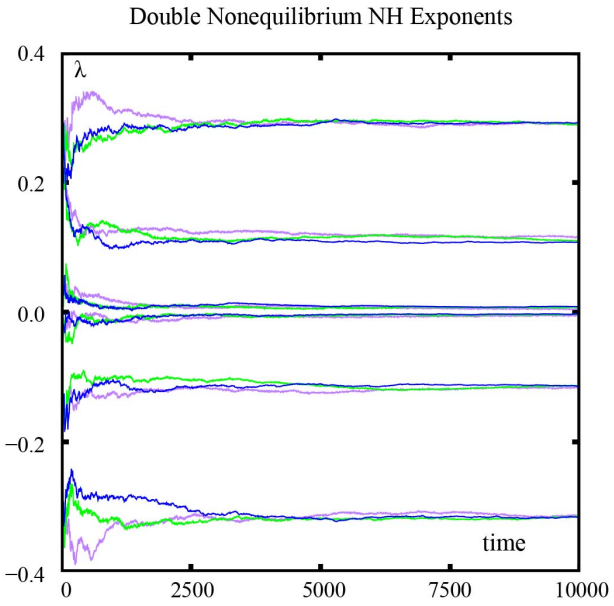

Fig. 9. A longer run, with as many as ten million timesteps ($dt = = 0.001$), suggests that visual convergence of the spectrum is complete at a time of a few thousand, a few million timesteps. Here the horizontal and vertical temperatures are controlled differently, at 1/2 and 2, respectively, with the temperatures permuted from those in Fig. 8. Evidently, there are two positive, two negative, and two vanishing exponents in these nonequilibrium problems. Permuting the initial momenta from $(0.6, 0.8)$ to $(0.8, 0.6)$ generates similar three-figure-averaged spectra for ten million timesteps, [0.292, 0.115, 0.005, −0.005, −0.116, −0.314]. Here, initially $p_x = 0.8,\ p_y = 0.6$

VI. Snook Prize 2024–2025

We wish to offer the Snook Prize of $1000 for the most interesting exploration and description of the nonequilibrium two-temperature cell model treatments obtained from extensions of Fig. 8. In particular, we would appreciate readers' efforts to understand the systematic dependence of the Lyapunov spectrum and fractal dimension on the magnitudes and differences of T_x and T_y. Entries should be submitted directly to CMST with referees selecting the winning contribution.

Acknowledgment

We are grateful to the Poznan Supercomputing and Networking Center affiliated with the Institute of Bioorganic Chemistry of the Polish Academy of Sciences for their support of these prizes honoring our late Australian colleague Ian Snook (1945–2013). We have appreciated several stimulating emails from Hesam Arabzadeh at the University of Missouri on the subject to this work as well as Kris Wojciechowski's encouragement. Kris also pointed out his investigation of the hard-disk cell models in 1982 [15].

References

[1] B.J. Alder, T.E. Wainwright, *Molecular Motions*, Scientific American **201**(4), 113–126 (1959).

[2] B.J. Alder, W.G. Hoover, T.E. Wainwright, *Cooperative Motion of Hard Disks Leading to Melting*, Physical Review Letters **11**, 241–243 (1963).

[3] S. Nosé, *A Unified Formulation of the Constant Temperature Molecular Dynamics Methods*, The Journal of Chemical Physics **81**, 511–519 (1984).

[4] S. Nosé, *A Molecular Dynamics Method for Simulations in the Canonical Ensemble*, Molecular Physics **52**, 255–268 (1984).

[5] Wm.G. Hoover, *Canonical Dynamics. Equilibrium Phase-Space Distributions*, Physical Review A **31**, 1695–1697 (1985).

[6] Wm.G. Hoover, C.G. Hoover, *Comparison of Very Smooth Cell-Model Trajectories Using Five Symplectic and Two Runge-Kutta Integrators*, Computational Methods in Science and Technology **21**, 109–116 (2015).

[7] W.G. Hoover, H.A. Posch, B.L. Holian, M.J. Gillan, M. Mareschal, C. Massobrio, *Dissipative Irreversibility from Nosé's Reversible Mechanics*, Molecular Simulation **1**, 79–86 (1987).

[8] B.L. Holian, W.G. Hoover, H.A. Posch, *Resolution of Loschmidt's Paradox: The Origin of Irreversible Behavior in Reversible Atomistic Dynamics*, Physical Review Letters **59**, 10–13 (1987).

[9] I. Shimada, T. Nagashima, *A Numerical Approach to Ergodic Problem of Dissipative Dynamical Systems*, Progress of Theoretical Physics **61**, 1605–1616 (1979).

[10] G. Benettin, L. Galgani, A. Giorgilli, J.M. Strelcyn, *Lyapunov Characteristic Exponents for Smooth Dynamical Systems and for Hamiltonian Systems; a Method for Computing All of Them. Part 1: Theory*, Meccanica **15**, 9–20 (1980).

[11] H.A. Posch, W.G. Hoover, *Chaotic Dynamics in Dense Fluids*, [In:] *Proceedings of the Physics of Fluids Conference at Calabria*, Lawrence Livermore National Laboratory Report UCRL–97344 - DE88 002453, Italy (1987).

[12] W.G. Hoover, E. Craig, H.A. Posch, B.L. Holian, C.G. Hoover, *Heat Transfer Between Two Degrees of Freedom*, Chaos **1**, 343–345 (1991).

[13] W.G. Hoover, H.A. Posch, L.W. Campbell, *Thermal Heat Reservoirs via Gauss' Priinciple of Least Constraint; Dissipation, Chaos, and Phase-Space Dimensionality Loss in One-Dimensional Chains*, Chaos **1**, 325–332 (1993).

[14] J. Kaplan, J. Yorke, *Chaotic Behaviour of Multidimensional Difference Equations*, [In:] *Differential Equations and the Approximation of Fixed Points*, Lecture Notes in Mathematics **730**, 228, Eds. H.O. Peitgen, H.O. Walther, Springer-Verlag, Berlin (2006).

[15] K.W. Wojciechowski, P. Pierański, J. Malecki, *A Hard-Disk System in a Narrow Box. 1. Thermodynamic Properties*, Journal of Chemical Physics **76**, 8170–8175 (1982).

Bill and Carol Hoover met in 1973 in Livermore California. Bill was a Professor with a joint appointment teaching courses in the University of California's Department of Applied Science at the Davis Campus' Livermore Branch while serving as a physicist at the Livermore Laboratory. Carol was a student at the Department and a plasma physicist at the Livermore Laboratory. Carol earned her PhD in 1978. A decade later the Hoovers reconnected socially and married in preparation for joint sabbatical work with Shuichi Nosé, Taisuke Boku, and Toshio Kawai at the Yokohama Campus of Keio University. They developed million-atom molecular dynamics simulations at Keio and continued small-system work with Brad Holian at Los Alamos and Harald Posch at the University of Vienna. The Hoovers have published hundreds of research papers in computational statistical mechanics and eight books, beginning with *Molecular Dynamics* in 1986 and most recently, in 2023, *Elegant Simulations, from Simple Oscillators to Many-Body Systems*, coauthored with Clint Sprott (University of Wisconsin) in 2023. The Hoovers moved from California to Nevada in 2005, and have continued their research work in retirement there in the ranching settlement of Ruby Valley in Elko County.